SIMS investigation of electron-beam damage to hydrous, rhyolitic glasses: Implications for melt inclusion analysis

MADELEINE C.S. HUMPHREYS,* STUART L. KEARNS, AND JON D. BLUNDY

Department of Earth Sciences, University of Bristol, Wills Memorial Building, Queen's Road, Bristol, BS8 1RJ, U.K.

ABSTRACT

Electron-beam irradiation causes permanent damage to hydrous, silica-rich glasses. The extent of electron-beam damage is quantified using data generated by SIMS analysis of points subjected to previous electron microprobe analysis (EPMA). Even optimum EPMA conditions cause damage to the glass, manifest as a marked depletion in alkali ions at the surface of an irradiated sample. Deeper in the sample, an enrichment in alkali ions to above-baseline levels is followed by a decay back to baseline. The depth of the final decay correlates with species diffusivity and increases in the order K-Li-Na. H-bearing species are also affected by electron beam irradiation, but in the opposite sense to the alkalis, i.e., they are enriched at the surface. Migration of alkaline earth cations is not observed because of their low diffusivities. Ion depletion or enrichment results from simple migration of ions toward or away from electrons implanted by the beam. Migration depth depends on species diffusivity and heating caused by the electron beam, and therefore increases with increasing electron beam current. Because of the reverse behavior of H, the mobile hydrous species in the presence of an electric field is probably OH^-. The extent of electron beam damage to glasses may increase with total water content. Critically, SIMS measurements of H, Li, Na, D/H, and $^6Li/^7Li$ after electron-probe analysis are compromised by the damage. Despite the damage caused by the electron beam, use of appropriate electron-beam conditions (e.g., 2 nA, 15 kV) gives volatiles by difference accurate to ~0.6 wt%.

Keywords: Electron-probe microanalysis, rhyolite glass, melt inclusions, secondary ion mass spectrometry, diffusion

INTRODUCTION

The analysis of hydrous, silica-rich glasses (e.g., tephra or melt inclusions in phenocrysts) can provide a wealth of petrological information. For example, melt inclusions can provide a direct measure of the pre-eruptive volatile contents of the liquid in which crystallization occurred. Increasingly, analysis of light isotopes and trace elements (e.g., D/H, $^6Li/^7Li$, B, Be) in melt inclusions are used to investigate magmatic processes. The small size of typical melt inclusions (20–40 μm) means that micro-analytical methods must be used. These include secondary ion mass spectrometry (SIMS), Fourier-transform infrared spectroscopy (FTIR), and electron probe micro-analysis (EPMA). While both SIMS and FTIR can be used to determine different volatile species (H_2O, CO_2) directly, EPMA can only be used to estimate total volatiles using the by-difference method. Despite this, EPMA is often the analytical method of choice, because of the ease of sample preparation, quick analysis time, accessibility and ease of use, relatively low cost, and because EPMA is used anyway to determine the major element composition. Using EPMA, large populations of melt inclusions can be "screened" for major element composition and volatiles-by-difference (VBD), prior to further investigation by SIMS or FTIR. However, insufficient attention has been paid to ensuring that the initial EPMA analysis does not affect subsequent micro–analytical work. In particular, a long-standing problem in electron microprobe analysis of hydrous, silica-rich glasses is sample damage caused by the electron-beam, resulting in compositional changes. The greatest problems are presented by Na and other alkalis, because they are mobile under the beam. This loss of Na X-ray intensity during irradiation has long been recognized (e.g., Lineweaver 1963; Goodhew and Gulley 1974; Autefage and Couderc 1980; Nielsen and Sigurdsson 1981; Spray and Rae 1995) and is thought to be a result of electric field-assisted diffusion (e.g., Usher 1981; Miotello and Mazzoldi 1982; Jbara et al. 1995). Moreover, the migration is known to be permanent and irreversible after irradiation ceases (Autefage and Couderc 1980). Neither the amount of damage, nor the error potentially resulting from electron-beam irradiation, has yet been quantified. Two questions remain to be answered:

(1) What is the reliability of the VBD obtained by EPMA?

(2) If damage is irreversible, what is the extent of the damage and how are future analyses, e.g., by SIMS, of the same point compromised?

To assess the reliability of VBD, we must first understand the processes involved in the second question. In this study we use SIMS to quantify the extent of damage caused to hydrous glasses by EPMA, paying specific attention to the alkali metals (Li, Na, K) and H. The main focus of the study is to investigate the influence of the electron-beam conditions and glass H_2O content on the extent of damage. We then use this information to address the reliability of VBD of hydrous, silica-rich glasses.

* E–mail: madeleine.humphreys@bristol.ac.uk

EXPERIMENTAL METHODS

Electron microprobe methods

In the first part of the experiment, samples of homogeneous glass were irradiated with an electron-beam using a CAMECA SX-100 5-spectrometer instrument. Each sample was carbon coated to a standard thickness of 15 nm and exposed to the beam for 4 min to simulate a typical quantitative electron microprobe analysis. A beam diameter of 15 µm was maintained, but beam conditions and glass composition were varied systematically. To assess the effect of changing beam conditions, Lipari glass was irradiated with electron beam currents of 2 to 40 nA, and accelerating voltages of 15 to 25 kV. To assess the effects of glass composition, we compared standard glasses with different major element contents (Lipari, Run121, and Run9) or H_2O contents (Lipari and MI514), irradiated at 15 kV and 2 nA or 10 nA. Table 1 gives the compositions of the glass standards used.

Secondary ion mass spectrometry

In the second part of the experiment, SIMS analyses were obtained of the electron–irradiated areas. The carbon coat was removed by brief polishing and the samples were sputter–coated with Au for a period of 200 s, equating to a coat thickness of approximately 20 nm. First, a non–irradiated area of each glass was analyzed, to provide baseline values for each sample Then, for each of the experimental conditions, the SIMS beam was manually aimed on the EPMA spot, which was usually easily visible using an inclined, reflected light microscope, with a 1.7 mm field of view attached to the instrument. The ion beam therefore sputtered down through the irradiated volume, thus collecting depth information about the altered glass chemistry. Any charging effects resulting from the SIMS beam would be the same for analyses in any one sample composition, under identical SIMS analysis conditions. We therefore normalized each SIMS profile to the baseline profile for that glass composition; this effectively removes any potential charging or matrix effects.

SIMS analyses were performed using a CAMECA ims-4f, controlled by Charles Evans and Associates PXT interface and software. A 3 nA O^- primary beam was accelerated onto the sample surface with a net impact energy of 14.5 kV. The focused beam was finely rastered to 5 µm to minimize potential charging effects. The secondary ions were extracted at +4.5 keV energy, with a 75 eV offset and ±20 eV energy window. Mass 4.5 was analyzed to monitor the background count rate of the electron multiplier detector. In each cycle, $^1H^+$, $^7Li^+$, $^9Be^+$, $^{23}Na^+$, $^{26}Mg^+$, $^{30}Si^+$, $^{39}K^+$, and $^{42}Ca^+$ counts were collected for 1, 5, 5, 3, 5, 2, 5, and 3 s respectively. Higher masses could not be analyzed concurrently with ^1H because of magnet hysteresis. ^{23}NaO counts were calculated from the measured Na counts, using the relative abundance of the ^{23}Na isotope and MO/M ratios from Hinton (1990). This interference with ^{39}K was found to account for <0.1% of the total ^{39}K counts. The number of cycles counted ranged from 30 to 80, corresponding to a counting time of ~30 to 80 min. Counting continued until a smooth, flat profile was obtained in all elements. To remove the effects of small variations in beam current, data are presented Si-normalized.

Secondary ions were sputtered continuously during analysis, thus generating depth profiles for each element. The mass spectrometer was calibrated for the analyte secondary ions prior to each analysis. This equated to an effective pre-sputtering period of less than 30 s. Assuming that the sputter rate did not vary during the analysis, cycle number corresponds directly to depth. Crater edge effects were not accounted for. SIMS pit depths were measured using a Tencor Instruments stylus profilometer. The profilometer was calibrated on a standard of etched quartz from VLSI standards. From multiple measurements, precision was ±0.0045 µm (2σ) and the instrument was found to be accurate to 0.008 µm. Smaller SIMS pits were measured and used to calibrate the depths of larger pits, assuming constant sputter rate. Pit depths varied from 2.050 to 5.467 µm. Pits were approximately the same width at the surface as the electron-probe spot (15 µm).

RESULTS

SIMS data are presented as counts per second (CPS) per isotope, normalized to Si (CPS), thus removing most irregularities resulting from small fluctuations in beam current during the analysis. Data for each sample are then normalized to the Si-normalized baseline analyses for that sample, to facilitate comparison between different elements and samples, and to
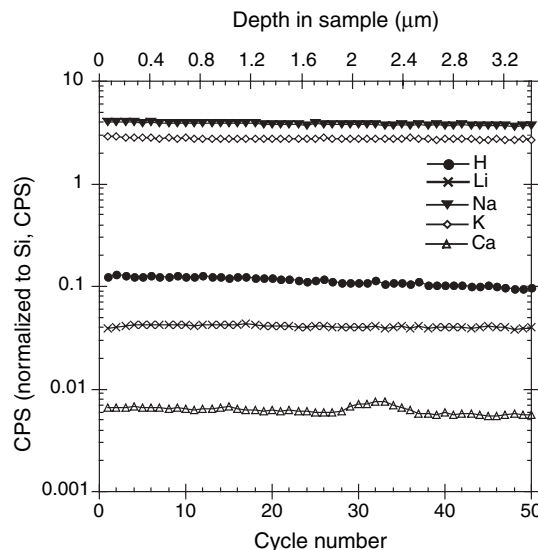
TABLE 1. Major element and water speciation data for hydrous glass standards used in EPMA experiments

Name	Run9*†	Run121‡	MI514§	Lipari‖#
Composition	Andesite	Dacite	Rhyolite	Rhyolite
Analysis	EPMA	EPMA	EPMA	XRF
No. analyses	34	10	11	
wt% oxide				
SiO_2	57.41[39]	67.38 [73]	71.01 [39]	74.03
TiO_2	0.97 [04]	0.62 [04]		0.08
Al_2O_3	16.79 [15]	14.66 [17]	9.71 [14]	12.72
FeO^T	4.79 [36]	4.49 [13]	3.87 [20]	1.56
MnO	0.14 [03]	0.00		0.08
MgO	3.12 [20]	1.28 [03]		0.00
CaO	6.83 [18]	2.2 [07]	0.20 [03]	0.72
Na_2O	3.90 [18]	2.65 [07]	5.40 [12]	4.06
K_2O	1.25 [06]	1.66 [03]	4.43 [10]	5.18
P_2O_5	0.30 [03]	0.01 [01]		0.00
LOI				1.04
F			0.14	
Cl			0.23	
Total	95.50	94.95	94.62	99.98
Water Speciation (FTIR)				
$H_2O_m - 5200 cm^{-1}$	2.51 [45]			0.126 [003]
$OH^- - 4500 cm^{-1}$	1.72 [19]			0.59 [01]
$H_2O_m - 1630 cm^{-1}$	2.52 [23]			
H_2O (a)	4.29 [27]	4.48 [27]	5.27 [06]	0.72 [01]
H_2O (b)	4.24 [35]			
ASI	0.83	1.44	0.69	0.94
Ca/(Na+K)	1.33	0.51	0.02	0.08

Notes: H_2O_m is average concentration of dissolved molecular water, based on 5200 cm^{-1} absorbance. (a) Total H_2O based on summation of OH^- and H_2O_m (5200 cm^{-1}). (b) Total H_2O based on summation of OH^- and H_2O_m (1630 cm^{-1}). Values in brackets represent 1 s.d., in terms of the least significant digit. ASI (Alumina saturation index).
* Mandeville et al. (2002).
† Manometry gave 4.32 wt% H_2O.
‡ Unpublished data, C. Mandeville.
§ Mayor Island rhyolite, New Zealand: Barclay (1995).
‖ Cannetto Lami lava, Lipari: XRF data from Sparks, R.S.J. (written communication).
H_2O data from Brooker, R.A., written communication.

FIGURE 1. Chemical profiles for H (filled circles), Li (crosses), Na (filled triangles), K (open diamonds), and Ca (open triangles) in Lipari glass, not previously irradiated by the electron beam. This analysis represents the baseline chemical profiles for Lipari. Data are normalized to Si (CPS) to remove small irregularities due to fluctuations in beam current. The small blip in Ca/Si at cycles 29–36 probably represents a tiny plagioclase microlite.

remove any matrix or charging effects. Figure 1 shows baseline chemical profiles in Lipari, i.e., profiles of an area of the glass that had not been irradiated with the electron beam. In this baseline analysis, chemical profiles for each element are flat and uniform with depth, indicating that the glass is chemically homogeneous.

Effect of changing electron beam conditions

The main features of electron beam damage are visible in Figure 2, which shows chemical profiles for Lipari after irradiation by a 15 kV, 40 nA electron beam. Alkaline earth element (e.g., Ca) profiles (not shown) are flat and uniform with depth, as in Figure 1. Alkalis (Li, Na, and K) all show a depletion in the first few cycles (at shallow depths in the sample), with very low initial count rates. Count rates then increase steeply and reach a slight peak before flattening off to baseline levels. The depth of the point at which the count rate profile crosses the baseline

varies between species, and is K << Li < Na. In contrast to the alkali metals, H has above–baseline count rates in the first few cycles of the analysis, thus showing the opposite behavior of the alkali metals.

The effects of increasing the electron beam current are seen in Figure 3, which shows Lipari irradiated by a 15 kV beam with 40, 10, or 2 nA beam current. As the beam current is increased, the extent of the initial alkali depletion increases, as does the depth at which count rates cross baseline levels. In the highest beam current experiment, the uppermost part of the damaged section is almost completely depleted in Li and Na, at around 5 to 10% of the baseline concentration. The extent of enrichment of H also increases with beam current. At the surface of Lipari in the lower beam current experiments, H counts show an exponential decrease to baseline levels. This is typical of surface contamination at low H_2O contents, but the feature is not seen in the 40 nA condition.
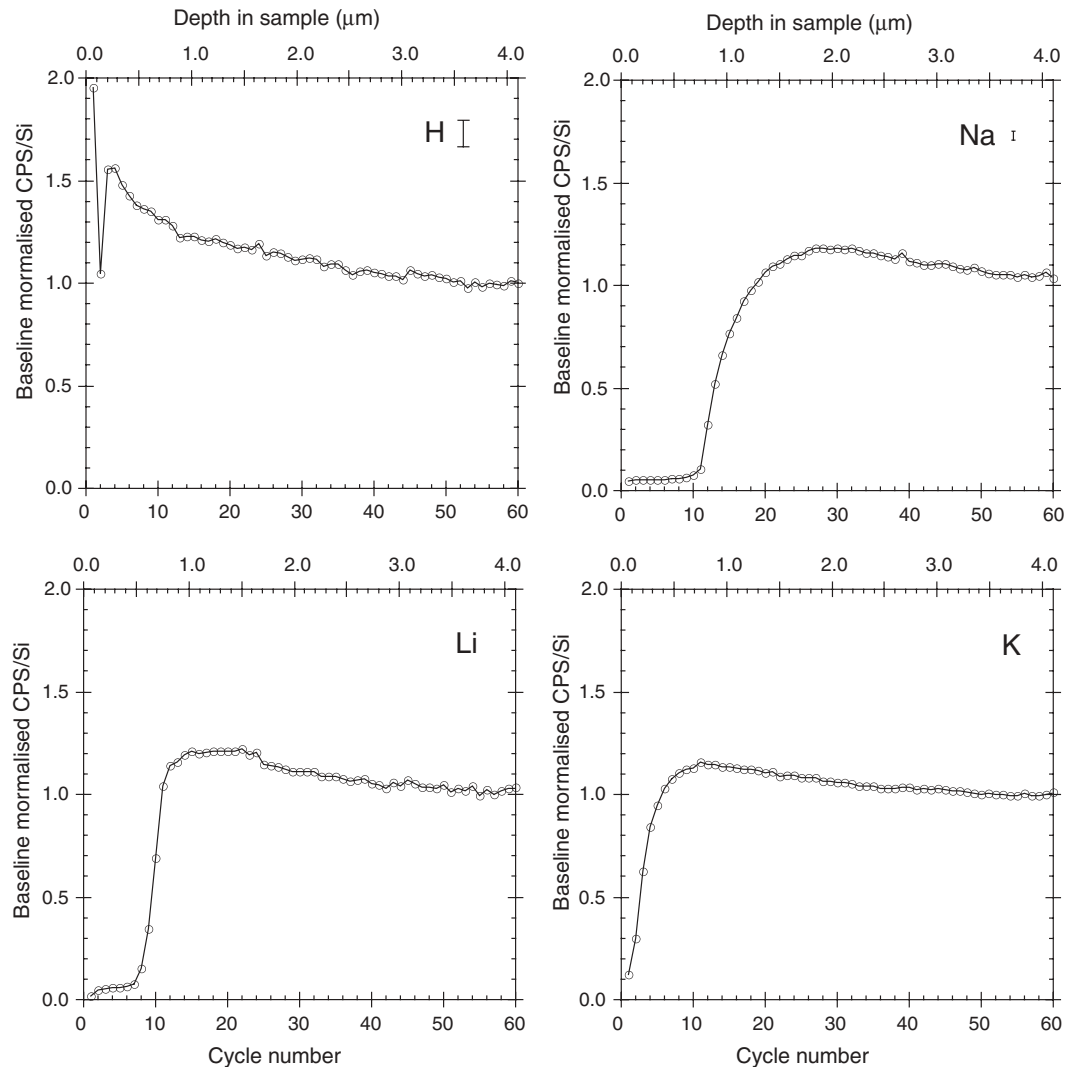

FIGURE 2. Chemical profiles for H, Li, Na, and K in Lipari irradiated by a 15 kV, 40 nA electron beam. Data are presented as baseline-normalized CPS/Si, to remove irregularities due to fluctuations in beam current. Baseline values are those shown in Figure 1. Counting errors are given as vertical bar, or are less than the size of the marker.
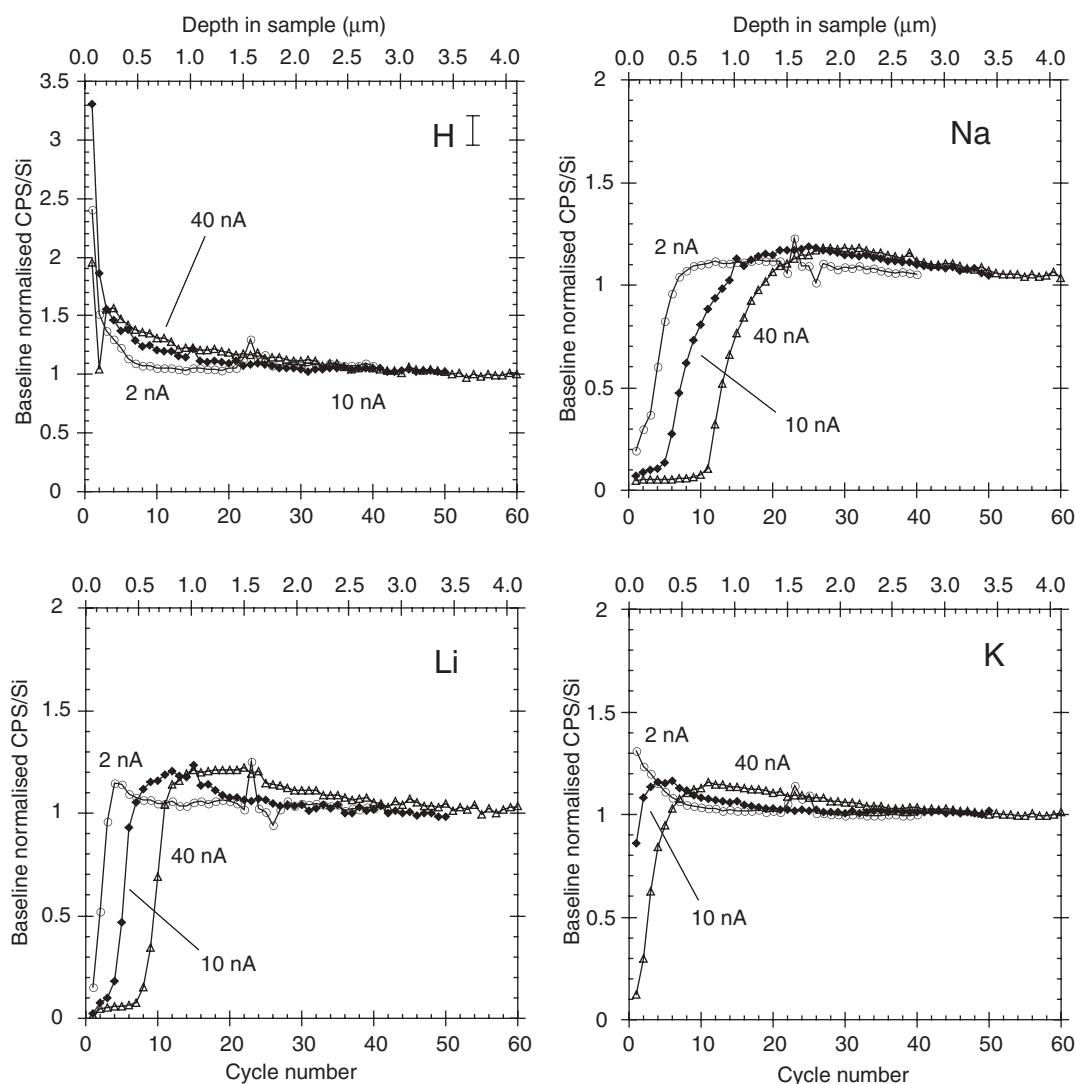
FIGURE 3. Chemical profiles for H, Li, Na, and K in Lipari irradiated by an electron beam with a 15 kV accelerating voltage and a beam current of 40 nA (open triangles), 10 nA (filled diamonds), or 2 nA (open circles). Data are presented as in Figure 2.

This is because damage from the higher current electron beam is sufficient to disguise any contamination effects from sample preparation. This implies that contamination occurred during polishing and sample preparation prior to EPMA. K also shows an exponential decrease in count rates at the surface, in the lowest current experiment. Given the similarity with the pattern of H counts, this is most likely also explained by surface contamination.

Overall, the effect of increasing the electron beam accelerating voltage is small (Fig. 4). Initially, increasing the accelerating voltage slightly increases the extent of alkali depletion and H enrichment at shallow depths in the sample. There is little difference between the 20 and 25 kV experiments, and in some elements count rates are less depleted (or enriched) under 25 kV than 20 kV (e.g., Li, H). Small perturbations in count rates at cycles 22–26 are probably due to fluctuations in SIMS primary beam current.

Effect of water content of the glass

Figure 5 shows chemical profiles for Lipari (0.7 wt% H_2O) and MI514 (5.27 wt% H_2O) (see Table 1 for major element composition), irradiated by a 15 kV, 2 nA electron beam. The relative extent and depth of depletion of alkali metals and enrichment of H are clearly much greater in MI514. An upper layer, highly depleted in alkalis, forms in MI514, though not in Lipari at these beam conditions (compare Fig. 3).

Effect of glass bulk composition

We have not studied glasses with a sufficient diversity of bulk composition to shed much light on the effects of composition on alkali migration. However, we can make the following general observations based on our results. Figure 6 shows Lipari, Run121 and Run9 (see Table 1), irradiated under a 15 kV, 10 nA electron beam. The extent of surface depletion in alkalis, and the depth at
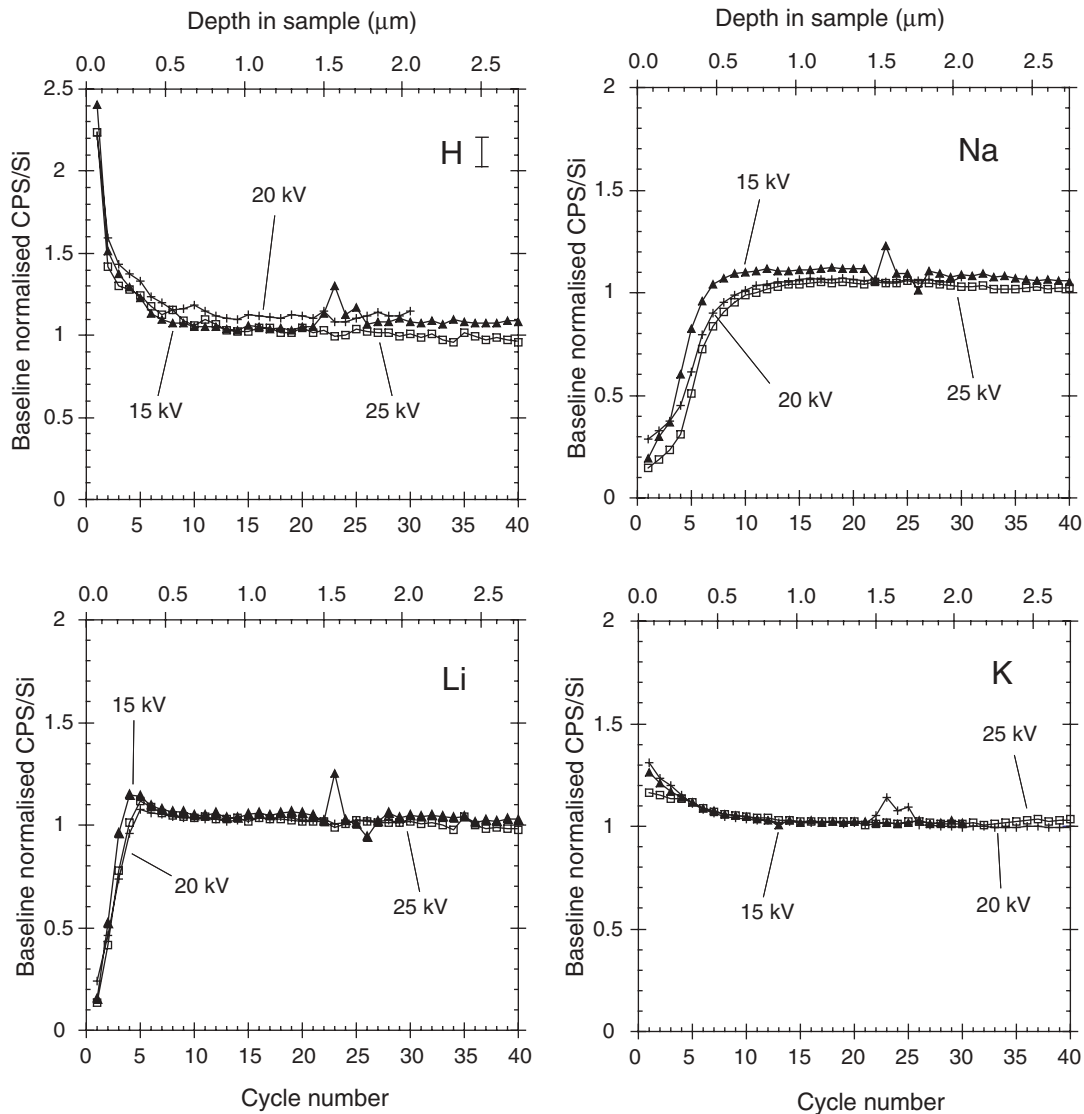
FIGURE 4. Chemical profiles for H, Li, Na, and K in Lipari irradiated by an electron beam with a 2 nA current and accelerating voltage of 25 kV (open squares), 20 kV (crosses), or 15 kV (filled triangles). Data are presented as in Figure 2. Exponential decrease in H/Si and K/Si is characteristic of surface contamination.

which count rates cross baseline levels, are again Na > Li >> K, and both increase as the ratio $Ca/(Na + K)$ of the glass decreases. There is no consistent correlation of the extent of depletion or the depth of recovery with ASI, total alkalis or H_2O contents. Damage is most extensive in Lipari, despite its much lower H_2O, high ASI and moderate total alkalis.

Summary

Surface depletion of all alkali metals is seen in glasses irradiated by an electron beam. The extent and depth of the depletion increases with increasing beam current and accelerating voltage. Damage is strongly affected by glass bulk composition. The depth also varies between species, but is always Na > Li >> K. In contrast to alkali metals, H counts show a surface enrichment.

DISCUSSION

Simple migration of ions

Figure 7 shows chemical profiles for the alkali ions in Lipari irradiated under beam currents of 40 to 2 nA, and accelerating voltages of 25 to 15 kV. The profiles clearly show movement of alkali ions from the upper parts of the sample during electron-beam irradiation. The depletions can be explained as the result of simple migration of ions by field-assisted diffusion (Miotello and Mazzoldi 1982). In this process, positively charged ions are attracted to electrons implanted at depth in the sample. Attraction occurs from all directions toward the electron implantation volume. Note that in experiments with the 20 kV accelerating voltage and 10 and 2 nA beams, the rate of recovery of alkali
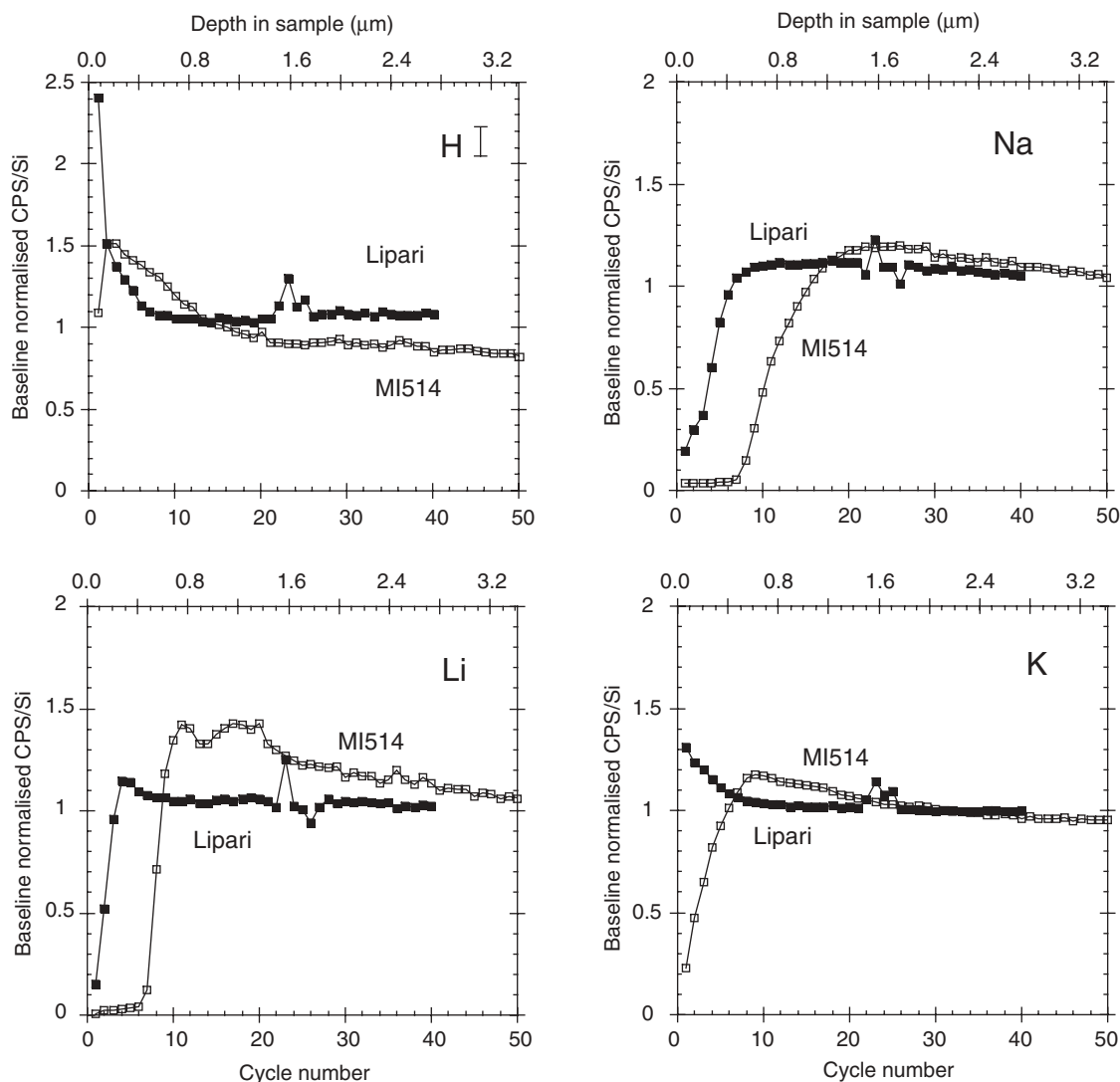
FIGURE 5. Chemical profiles for H, Li, Na, and K in Lipari (0.72 wt% H_2O, closed squares) and MI514 (5.27 wt% H_2O, open squares) irradiated by a 15 kV, 2 nA electron beam. Data are presented as in Figure 2.

count rates is much shallower than in other experiments. This may be because the SIMS beam did not coincide directly with the center of the EPMA spot. Migration occurs in 3-D but will be most intense vertically, along the axis of the electron beam, and much weaker laterally, near the edge of the implantation volume. A slightly off-axis SIMS analysis would therefore produce anomalous data.

Figure 8 shows a sketch of a typical chemical profile. Under a lower power electron beam (Fig. 8a), a depleted layer, Region Ia, forms at the surface, with a corresponding enriched layer (Region II) at depth. In experiments using a more powerful electron beam, a highly depleted layer (Region Ib) develops at the top of the sample (Fig. 8b). Almost all Na and Li ions have been removed from this layer. This observation supports work by Jurek et al. (1996), who noticed the creation of a compact, alkali-free surface layer, underlain by structurally deteriorated, "channelized" glass. At very powerful beam conditions, therefore, the surface layer

of the sample becomes so damaged that almost its entire alkali content is displaced deeper into the sample.

Assuming simple migration of ions, a mass-balance of the depleted volume (Region Ia) and the enriched volume (Region II) should show that the total number of ions displaced from Region Ia is equal to the number deposited in Region II. The problem is rather complex because the SIMS analysis samples a roughly cylindrical profile down through the electron-irradiated volume. In effect, chemical information from the SIMS analysis is radially averaged over this cylindrical profile. A full mass-balance would require information about the 3-D, un–averaged concentration profile for each species. Although there is a correspondence between the size of the depletion in Region Ia, and the size of the enrichment in Region II, a full mass-balance is not possible from the techniques used in this study.

We note that the shape of the measured chemical profiles cannot be explained by a purely electrostatic attraction. Under
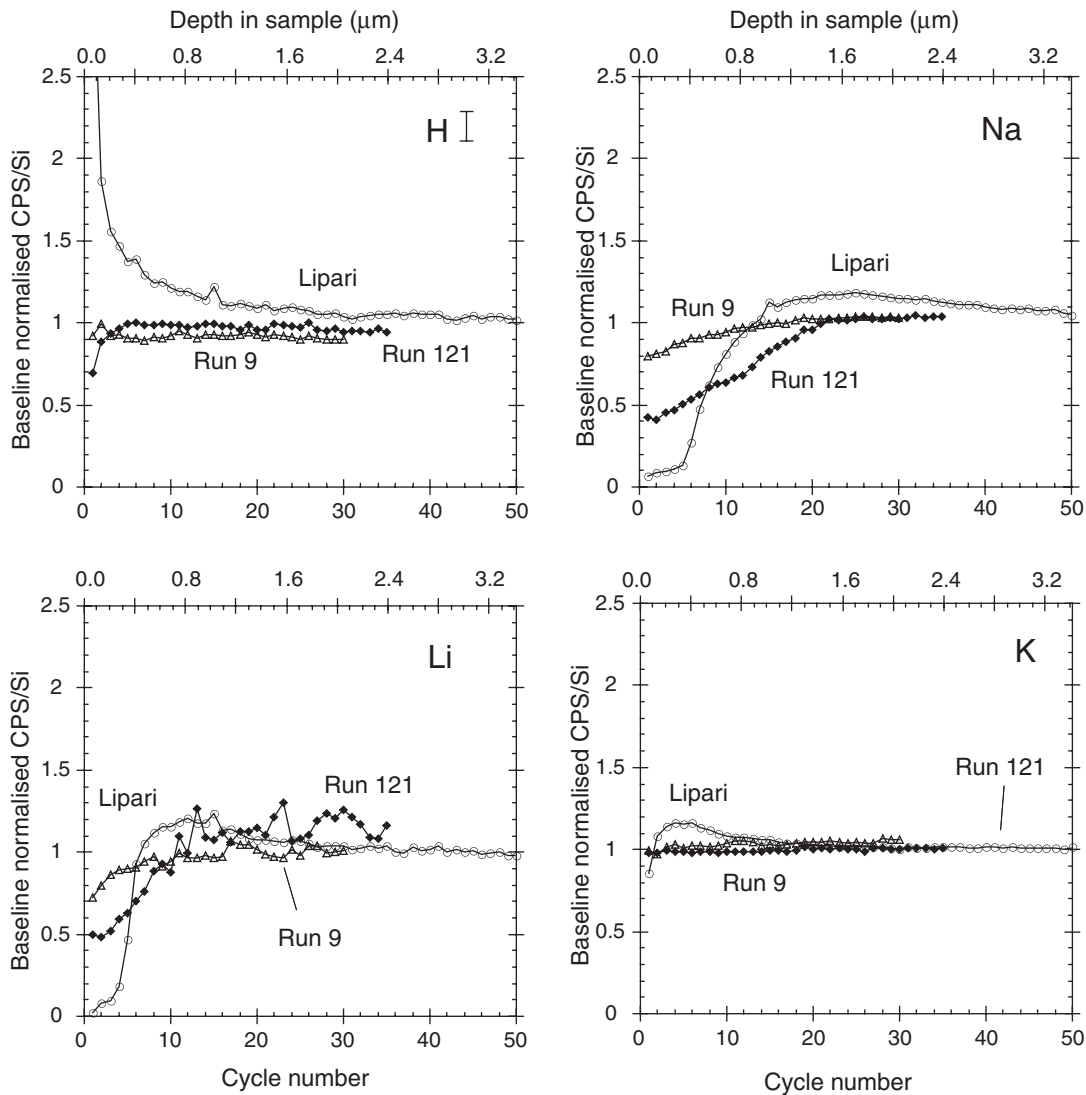
FIGURE 6. Chemical profiles for H, Li, Na, and K in Lipari (open circles), Run121 (filled diamonds), and Run9 (open triangles), irradiated by a 15 kV, 10 nA electron beam. Data are presented as in Figure 2.

purely electrostatic attraction, the force felt by the alkali ions would decrease away from the charge center (i.e., the depth of maximum implanted electron density). Ions close to the surface would feel a small force and would migrate weakly, compared with ions close to the implanted electrons, which would move much further. In contrast, the data show that surface ions are more strongly affected than those at depth. We therefore need to consider how migration will be affected by the extent and depth of electron implantation, and by any temperature effects caused by the EPMA beam. Note that, because the alkali ions are attracted toward the implanted electrons, we would expect that migration depth is always less than both electron penetration depth and the depth of the charge center.

Electron implantation

Electron penetration depth or range can be calculated according to Kanaya and Okayama (1972):

$$R_{KO} \ (\mu m) = \frac{0.0276 A \cdot E_o^{1.67}}{Z^{0.89} \rho} \qquad (1)$$

where R_{KO} is the range, A = atomic mass (g/mol), Z = atomic number, ρ = density (g/cm^3), and E_o = beam energy (keV). Table 2 gives calculated penetration depths for Lipari, Run121, and Run9, for beam energies of 15, 20, and 25 keV. In each case, migration depth is less than penetration depth.

The program *Casino* (Hovington et al. 1997) can be used to produce Monte Carlo simulations of electron trajectories and electron depth distribution. Figure 9 shows simulations based on the composition and density of Lipari glass, for a variety of beam conditions. The simulations show that both electron penetration depth and the depth of the charge center (maximum electron density) increase with electron-beam accelerating voltage. In addition, the maximum dimension of the irradiation volume increases as accelerating voltage increases. The strength of the
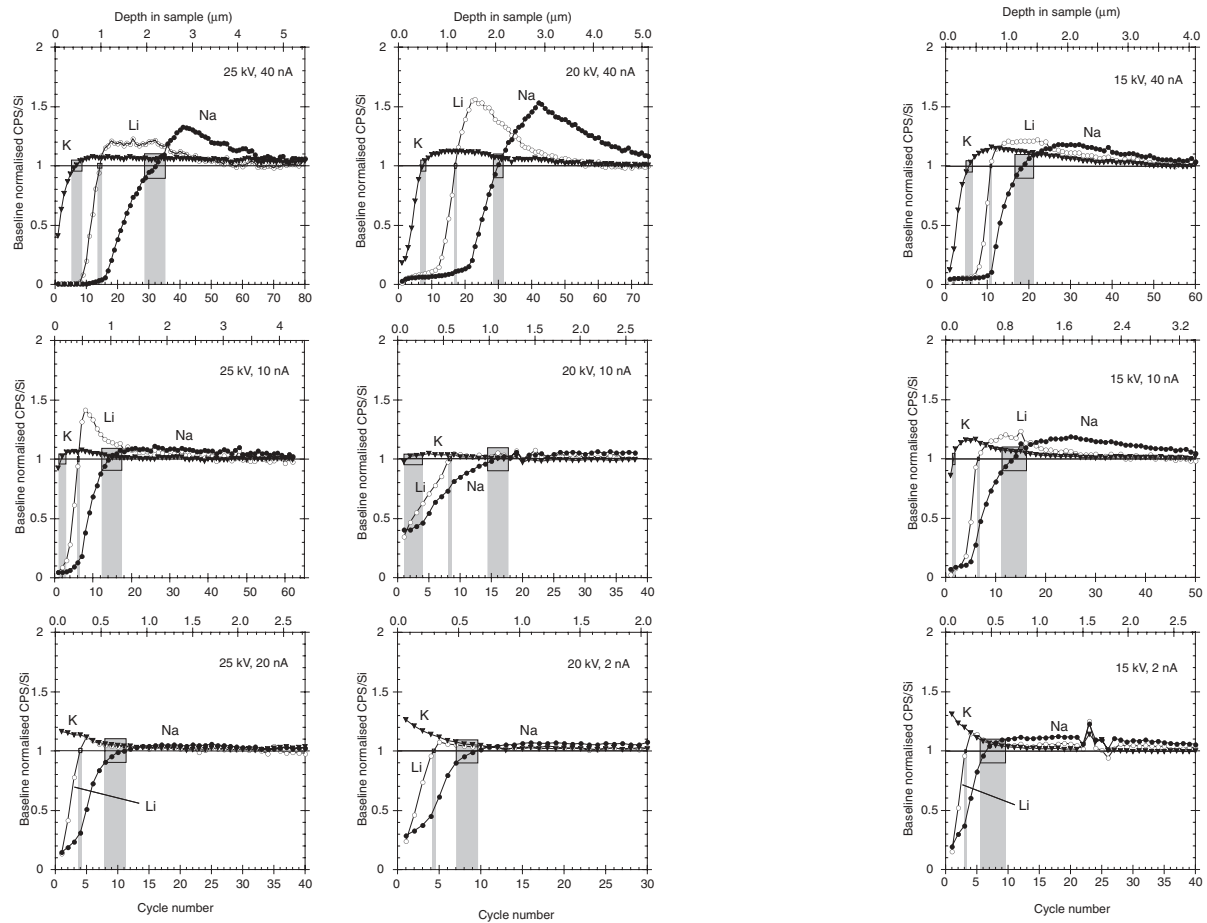
FIGURE 7. Chemical profiles for Li, Na, and K in Lipari, irradiated under beam currents of 2 to 40 nA, and accelerating voltages of 15 to 25 kV. Horizontal line at (CPS/Si) = 1 represents Lipari baseline concentrations. The migration depth, Z_0, is the point where the profile crosses this line. Black boxes around Z_0 mark the error in determining Z_0 for each element (based on errors in determining baseline, from counting statistics). Gray boxes show errors in Z_0 extended to cycle number (depth) axis (see also Table 3). Note variation of depth scale in each plot.

TABLE 2. Values of diffusion distances for migrating species in Lipari, under different electron-beam currents and accelerating voltages

Accelerating voltage (kV)	Beam current (nA)	R_{KO} (μm)	Simulated electron penetration depth (μm)	Depth of simulated maximum electron density (μm)	Measured migration depth, Z_0, (μm)						Temperature estimated from diffusion data (°C)						T_{VC} (°C)
					Li	± err	Na	± err	K	± err	Li	± err	Na	± err	K	± err	
25	40	6.4	5.7	4.1	0.99	0.03	2.2	0.2	0.48	0.10	273	2	290	4	375	13	35.2
25	10	6.4	5.7	4.1	0.41	0.02	1.0	0.2	0.14	0.07	226	2	245	8	306	19	23.8
25	2	6.4	5.7	4.1	0.27	0.02	0.6	0.2	–	–	206	4	221	13	<228	–	20.8
20	40	4.4	3.9	2.8	1.09	0.02	2.0	0.1	0.5	0.03	279	1	282	5	377	5	32.1
20	10	4.4	3.9	2.8	0.57	0.02	1.1	0.1	0.17	0.10	242	2	248	5	315	24	23.0
20	2	4.4	3.9	2.8	0.29	0.02	0.6	0.1	–	–	210	3	214	8	<228	–	20.6
15	40	2.8	2.4	1.9	0.75	0.02	1.3	0.2	0.38	0.07	256	3	258	8	360	11	29.1
15	10	2.8	2.4	1.9	0.44	0.02	1.0	0.2	0.10	0.02	229	2	241	10	290	8	22.3
15	2	2.8	2.4	1.9	0.22	0.02	1.0	0.1	–	–	197	4	208	10	<228	–	20.5

Notes: R_{KO} is the Kanaya-Okayama electron penetration range (Kanaya and Okayama 1972). Simulated electron penetration depth and depth of maximum electron density are simulated using CASINO (Hovington et al. 1997). Temperatures estimated from diffusion data (Eqs. 2 and 3) use data from Jambon (1983). T_{VC} is from Vassamillet and Caldwell 1969 (Eq. 4). Migration depths are measured from chemical profiles. Thermal conductivity of rhyolite = 0.014 W·cm⁻¹·K⁻¹ (Handbook of Chemistry and Physics). See text for details.

electrostatic attraction felt at the surface will therefore *de*crease with increasing accelerating voltage. This implies that the amount of diffusion would decrease at higher accelerating voltages. However, the decrease in diffusion caused by decreasing electrostatic field strength is balanced by enhanced diffusion caused by enhanced sample heating (see below). This trade-off between electrostatic field strength and temperature was recognized by Goodhew and Gulley (1974), over a wider range of accelerating voltages, and explains the subtle effect of changing the beam accelerating voltage (Fig. 4).
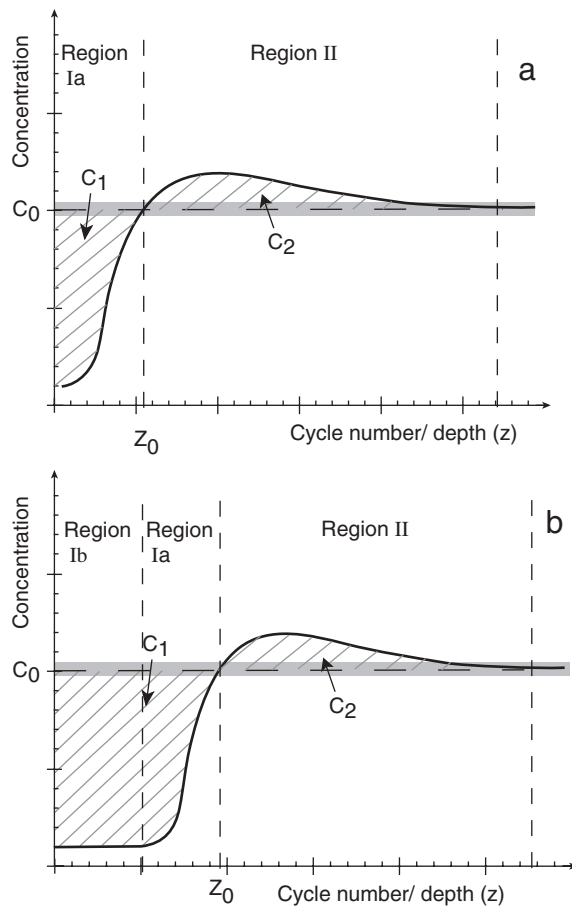
FIGURE 8. (**a**) Theoretical chemical profile after simple migration of alkali ions. C_0 represents the baseline concentration. Under simple migration, the number of ions displaced (C_1) is equal to those deposited (C_2), producing a depleted layer (Region Ia) and an enriched lower layer (Region II). Z_0 marks the point at which the profile crosses the baseline, i.e., where gain of ions from above is matched by loss of ions to greater depth. (**b**) Under high power electron-beam irradiation, Region Ia becomes stable at ~0.5 to 5% of its original alkali contents, and Region Ib develops.

Temperature effects of the beam

The migration depth can be measured from each chemical profile, and is defined here as Z_0, or the point at which the profile crosses the baseline (Fig. 8), where gain of ions from above is matched by loss of ions below. Under field-assisted diffusion, the ion migration depth will vary according to the diffusivity of the ion species and the strength of the force due to the electric field. Since the ion diffusivity is strongly dependent on the temperature, we can estimate the extent of heating caused by the beam by evaluating the amount of diffusion undergone by each ion.

Ion diffusivity can be calculated using the expression:

$$D_i = D_{o,i} \exp\left(-\frac{E_a}{RT_{diff}}\right) \tag{2}$$

where $D_{o,i}$ is a pre-exponential constant for the ion (i) of interest, E_a is the activation energy, T_{diff} is the temperature at which diffusion is occurring and R is the universal gas constant. Diffusivities

are taken from Jambon's (1983) data for Iceland obsidian.

The migration depth, Z_0, is equivalent to the diffusion distance:

$$Z_0 = \sqrt{D_i t} \tag{3}$$

where t is the analysis time. We can therefore use Z_0 to calculate D_i, and hence T_{diff}. There are various assumptions and caveats with this approach. First, and most importantly, the method does not take into account the variation of the strength of electrostatic attraction with depth. The strength of electrostatic attraction will also vary with accelerating voltage as previously discussed. However, any change in migration distance with beam current, at constant accelerating voltage, will give a measure of heating effects. Second, diffusivity data are for dry obsidian, while addition of H_2O may greatly increase diffusivities. Finally, the temperature estimated must be the average temperature *over the total distance diffused* by the ion, and therefore less than $T_{surface}$.

We can compare T_{diff} with temperatures calculated from empirical relationships. An empirical method for estimating the amount of heating caused by the beam is put forward by Vassamillet and Caldwell (1969):

$$T_{VC} - T_o \cong \frac{W_o}{2\pi K r_o} \tag{4}$$

where W_o is the power input of the beam (watts); K is the thermal conductivity of the matrix (W·cm^{-1}·°C); r_o (m) is the radius of the hemisphere (which has equivalent volume to that of the irradiated disk, in the case where beam diameter is greater than the electron range); T_0 is the initial temperature and T_{VC} is the temperature at the surface of the equivalent hemisphere.

Table 2 gives migration depths measured from Figure 7, along with associated temperature estimates, and temperatures calculated using the empirical relationship in Equation 4. Where the chemical profile does not cross the baseline at all (e.g., K in experiments with the 2 nA beam), T_{diff} cannot be determined because surface contamination effects overprint any possible depletion curve. T_{diff} is probably not zero, so a maximum temperature is therefore calculated, assuming that the distance diffused is on the order of the depth errors (0.02 μm). Where chemical profiles are very flat and do not pass through the upper bound of the error box (e.g., Na, 25 kV/2 nA, 20 kV/10 nA, and 2 nA, see Fig. 7) the error box is extended only up to Z_0.

Table 2 shows that temperatures estimated using Li and Na diffusion are similar, but temperatures estimated using K diffusion are much higher. The depth of diffusion increases with beam current because, at constant accelerating voltage T_{diff} also increases with beam current (Fig. 10). Diffusion temperatures do not agree well with empirically calculated temperatures (200–380 °C, compared with 20–40 °C, respectively). However, this is because T_{VC} is the temperature at the edge of the irradiated volume, while T_{diff} is an average over the distance diffused by an ion. Electrons penetrating the sample have greatest energy near the surface, so the temperature increase will be greatest near the sample surface. The estimated temperatures and diffusion distances of the alkali ions therefore record the temperature–depth profile within the sample. Because diffusivity varies non–linearly with temperature, the region of high ion diffusion is
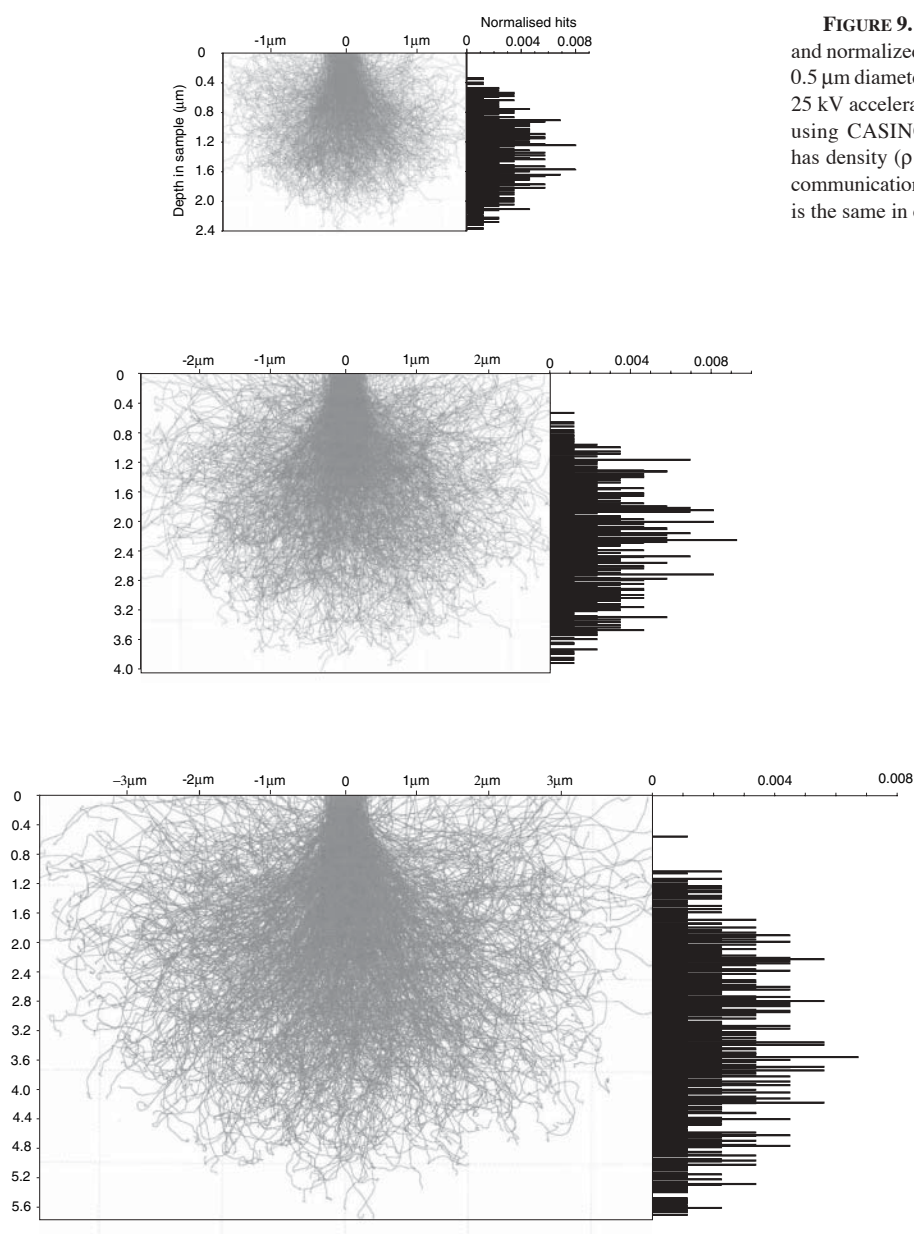
FIGURE 9. Monte Carlo simulations of trajectories and normalized depth distributions of electrons from a 0.5 µm diameter beam, with (**a**) 15 kV, (**b**) 20 kV, or (**c**) 25 kV accelerating voltage. Simulations are produced using CASINO (Hovington et al. 1997). Substrate has density ($\rho = 2.39$ g cm^{-3}, R.A. Brooker, personal communication) and composition of Lipari glass. Scale is the same in each figure.

confined to the upper parts of the sample where heating is most significant. The high near-surface temperatures are consistent with Hulinsky et al. (1996) and Borom and Hanneman (1967), who report maximum surface temperatures of over 1000 °C for some glasses.

Variations in species diffusivity can also explain the flat chemical profiles of the alkaline earth cations. Using Ca as an example, diffusion is orders of magnitude slower even than K. Diffusion data from Jambon (1983), shows that even at temperatures of 377 °C (the maximum temperature estimated from K diffusion), Ca ions would diffuse only 5.6×10^{-11} µm. The distances diffused are therefore much too small to be observed on the profiles.

The role of bulk composition

The stability of glass to electron bombardment depends on bulk composition because this determines its structural properties. Diffusivities of the mobile ions are determined by the degree of polymerization and are therefore affected by aluminosity (Mysen 1983) and alkali ion abundance (Shelby 1997), as well as by ionic radius (Jones 1971). Both the extent of alkali ion depletion (or H enrichment) and the depth at which count rates recover, are greater in MI514 than in Lipari. These two glasses have similar Na_2O and total alkali contents, but differ in H_2O, Ca/(Na + K) and ASI (Table 1). The difference in magnitude of electron beam damage may explained by the increase in ion diffusivities achieved by adding water to a melt or glass. For a given
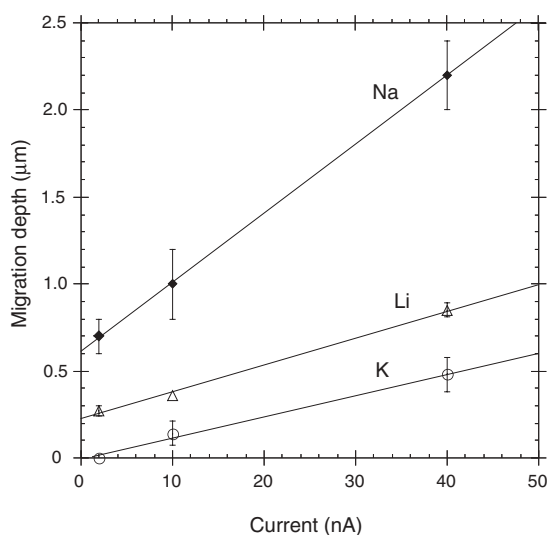
FIGURE 10. Variation of measured alkali (Li, Na, K) migration depth with electron-beam current. Regression lines are fitted with a linear least squares model. Alkali migration increases with beam current because the heating effect enhances diffusion. Alkali migration distances correlate with ion diffusivities, increasing in the order K-Li-Na.

set of beam conditions and bulk composition, ions would be able to move further in the H_2O-rich glass during the analysis time. An additional explanation lies in the bulk polymerization of the glass. The polymerization state of the glass is in part determined by the ASI, with higher values leading to more polymerized glass structures. ASI is lower for MI514 than for Lipari. However, ASI does not always correlate with increased sample damage: Run 9 is less damaged than Lipari (Fig. 6), although it has lower ASI and higher H_2O. One possible reason is that Run 9 has higher Ca/(Na + K). Divalent cations (e.g., Ca^{2+}) occupy interstices in the glass structure and thus reduce the diffusivity of mobile network modifiers such as Li^+ and Na^+ (Shelby 1997). Addition of H_2O and F may enhance this effect in MI514, as suggested by Morgan and London (2005). However, further investigation of more closely related glass compositions is required, to decouple reliably the effect of H_2O content from the effects of glass polymerization and structure.

The behavior of H_2O

H ions behave differently from the alkalis in that they are enriched at the surface of the sample in Region Ia, and depleted in Region II. This cannot be the result of any diffusive gradient of H_2O between the sample and the ion probe vacuum because each profile is normalized to the baseline analysis for that glass, so any such matrix effects would have been cancelled out. Instead, the enrichment implies that ions are diffusing *away* from the charge center rather than toward it. It is therefore very likely that a negatively charged species is diffusing, and so we suggest that OH^- is the mobile species. The extent of migration is therefore likely to be affected by water speciation in the glass, and also by total water content, since speciation changes with water content (Stolper 1982). However, the problem is further complicated, since it is known that diffusivities for H_2O increase

at higher total H_2O contents (Delaney and Karsten 1981). Zhang (1999) studied diffusivities of the different water species and found that only H_2O was mobile. However, his measurements were carried out in the absence of an electric field, and may not be relevant in this case. Species diffusivities in an electric field and at different H_2O contents are not known and we are therefore unable to test further the hypothesis that OH^- is the mobile species during EPMA.

IMPLICATIONS FOR MELT INCLUSION ANALYSIS

An electron–probe beam clearly has a strong, damaging effect on hydrous, Si-rich glasses. We must therefore ask how the extent of beam damage can be minimized. With the damage minimized, how reliable is the volatiles-by-difference obtained by EPMA? And what implications does the damage have for subsequent SIMS analyses?

Minimizing electron-beam damage

Previously, several authors have suggested empirical methods of reducing or correcting for alkali migration or diffusion during EPMA. There are three options:

(1) Reduce the temperature to the point where diffusion is minimal, (e.g., –190 °C, Kearns et al. 2002), by operating on a cryostage. This option works well because the diffusivities of the mobile species at cryogenic temperatures are so small that migration is insignificant, even in the presence of an electric field. However, cryostages are not routinely fitted to most modern electron microprobes.

(2) Obtain Na$K\alpha$ X-ray decay curves, and extrapolate back to the zero-time intercept to correct to initial Na concentrations (Nielsen and Sigurdsson 1981). A problem with this technique is that alkali metal decay undergoes an incubation period inversely proportional in length to the incident beam current. The extrapolation technique may therefore underestimate Na contents by up to 10% relative (Morgan and London 1996). Note that this technique does not mitigate alkali migration, it simply corrects for it. Thus, the effects on other mobile species not analyzed by EPMA (e.g., Li) cannot be corrected.

(3) Adjust the electron beam and analysis conditions to minimize alkali migration (e.g., Devine et al. 1995; Morgan and London 1996; King et al. 2002). Most authors recommend making various changes to the electron beam conditions to reduce alkali migration, such as reducing the beam current, increasing beam diameter, decreasing the accelerating voltage and reducing counting times. The trade–off is that counting statistics are worsened by these changes, particularly for minor to trace level components. However, for those users without access to a cryostage, adjusting beam conditions is the best method of reducing ion migration.

Reliability of VBD

We can use the SIMS experiments to assess the best electron-beam conditions for analysis of hydrous, silica-rich glasses. The SIMS data from the electron-irradiation experiments show a clear decrease in the extent of damage caused to the glass, as beam current was reduced. The least damage was caused during 15 kV, 2 nA experiments. We therefore analyzed a suite of hydrous, rhyolitic melt inclusions in plagioclase phenocrysts

TABLE 3. Calibration standards and analytical procedure for each element

Element	Primary standard	Conc. in standard (wt%)	Peak/bkg counting time (s)	Analysis order	Crystal (spectrometer)
Na	Albite	11.61	15/ 8	1	LTAP (1)
F*	Durango apatite	3.53	100/ 20	2	LTAP (1)
Ca	Wollastonite	48.01	40/ 20	1	PET (2)
Ti	$SrTiO_3$	43.54	40/ 20	2	PET (2)
S	Barite	27.45	30/ 15	3	PET (2)
K	Sanidine	13.64	40/ 20	1	LPET (3)
P	Durango apatite	40.77	80/ 20	2	LPET (3)
Si	KN18	74.60	30/ 15	1	TAP (4)
Al	Albite	19.65	30/ 15	2	TAP (4)
Mg	St. Johns Island Olivine	49.18	40/ 20	3	TAP (4)
Mn	Mn metal	100.00	60/ 20	1	LLIF (5)
Fe	St. Johns Island Olivine	9.55	60/ 20	2	LLIF (5)

* F peak search was done separately using a differential manual PHA and background positions of –500, +1000 from peak.

from Mount St. Helens (Blundy and Cashman 2005), using the same CAMECA SX-100 instrument, with a 2 nA, 15 kV primary beam, and 15 μm defocused beam. Na and Si were analyzed first and concurrently, with short counting times. The primary Si standard (KN18 glass, Nielsen and Sigurdsson 1981) was used because of its similarity with the unknown. Matrix correction was done online using a PAP correction (Pouchou and Pichoir 1984), calculating VBD (H_2O) by using H as a "difference element" and stoichiometric oxygen. Table 3 gives details of the primary standards and analytical procedures used for each element. Each analysis lasted approximately 4 min.

Figure 11 shows the results of VBD calculated from the electron-microprobe analyses, vs. H_2O measured using SIMS, on un-irradiated parts of the melt inclusions (n = 38). VBD and SIMS measurements agree well; a regression curve has gradient 0.99 (i.e., it lies on the 1:1 line) and $R^2 = 0.81$. A full propagation of the counting errors gives a *precision* for VBD of ±0.75 wt%, because of the decreased count rates at low beam currents. However, the absolute deviation from the expected (SIMS) values reflects the *accuracy* of the technique: the average absolute deviation (AAD) is 0.56 wt%. This study show therefore shows, in common with previous studies (e.g., Devine et al. 1995; Morgan and London 1996; Morgan and London 2005) that VBD is a reliable technique for giving total H_2O content for hydrous, Si-rich glasses to within ~0.6 wt%, provided that appropriate beam conditions are used. For hydrous, rhyolitic melt inclusions, we recommend 2 nA, 15 kV, and a 15 μm spot. It is anticipated that for glasses of different composition, different beam conditions may be preferred. At higher current densities, apparently "accurate" VBD may be an artifact of losses in Na and K being offset by Si and Al grow-in (Morgan and London 2005).

Implications for SIMS analysis of glasses

The inevitable electron-beam damage caused to hydrous glasses during EPMA will be reflected in subsequent SIMS analyses, regardless of the beam conditions used. This work shows that electron-beam damage from previous electron microprobe analysis may seriously compromise measurements for alkalis and H, and we speculate that similar effects might also be seen in light elements such as F and Cl. In the study of melt inclusions or tephra particles, SIMS is routinely used to measure the concentrations of light trace elements and volatile components not directly available from EPMA, e.g., Li and H_2O. Importantly, different isotopes may have different diffusivities, and would therefore be affected by electric field–assisted diffusion to varying extents.
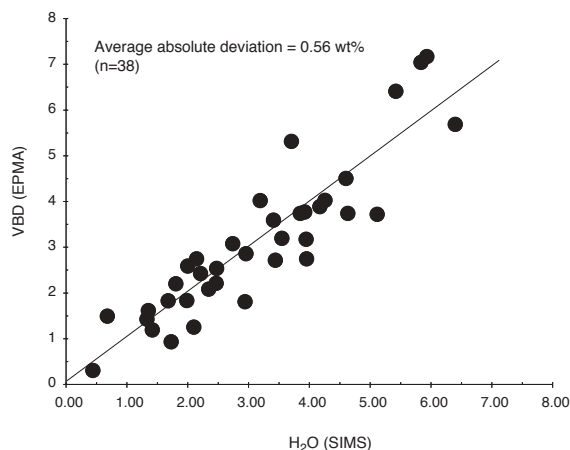

FIGURE 11. Volatiles by difference (VBD) measured using EPMA, vs. wt% H_2O, measured by SIMS. Number of analyses = 38; $R^2 = 0.81$. Average absolute deviation (AAD) from expected values = 0.56 wt%. Data are from Blundy and Cashman (2005).

SIMS analysis of geologically significant isotopic ratios, such as D/H or $^6Li/^7Li$, will therefore also be jeopardized.

Methods to mitigate the impact on SIMS analysis depend largely on melt inclusion or particle size. In a large inclusion, the SIMS analysis may be done on an undamaged area. However, in small inclusions the SIMS pit will be coincident with at least part of the EPMA spot, and ions will therefore be collected from the damaged area. Short SIMS analysis times will underestimate alkali count rates since they collect ions mainly from the depleted Region Ia. H count rates will therefore be overestimated since they are enriched in Region Ia. Similarly, analyses following substantial pre-sputtering (which is often used to remove surface contamination) will overestimate alkali count rates, since part of Region I has been removed and ions will be collected mainly from the enriched Region II. H counts would be underestimated since H is depleted in Region II. Note that if appropriate EPMA conditions have been used then it is unlikely that Region Ib will be present. SIMS analyses could be performed before EPMA; however there is then a risk that polishing to remove the SIMS pit could also remove the melt inclusion. In addition, EPMA is a useful tool for screening large populations of melt inclusions or tephra particles prior to SIMS analysis. Thus, if the SIMS analysis must be coincident with an EPMA spot, the analysis should be done with no pre–sputtering, and continued until all profiles reach baseline levels (flat, smooth curves). In that

case, because of the approximate conservation of mass during migration, averaging count rates over all cycles should equal the baseline concentration. Alternatively, SIMS data reduction should be performed using only the later cycles, after baseline levels have been reached.

REFERENCES CITED

Autefage, F. and Couderc, J.-J. (1980) Étude du mécanisme de la migration du sodium et du potassium au cours de leur analyse à la microsonde électronique. Bulletin de Minéralogie, 103, 623–629.

Barclay, J. (1995) The role of volatiles in the ascent and eruption of rhyolitic magmas. Ph.D. thesis, University of Bristol.

Blundy, J.D. and Cashman, K.V. (2005) Rapid decompression-driven crystallisation recorded by melt inclusions from Mount St. Helens volcano. Geology, 33, 793–796.

Borom, M.P. and Hanneman, R.E. (1967) Local compositional changes in alkali silicate glasses during electron microprobe analysis. Journal of Applied Physics, 38, 2406–2407.

Delaney, J.R. and Karsten, J.L. (1981) Ion microprobe studies of water in silicate melts. Concentration-dependent water diffusion in obsidian. Earth and Planetary Science Letters, 52, 191–202.

Devine, J.D., Gardner, J.E., Brack, H.P., Layne, G.D., and Rutherford, M.J. (1995) Comparison of microanalytical methods for estimating H_2O contents of silicic volcanic glasses. American Mineralogist, 80, 319–328.

Goodhew, P.J. and Gulley, J.E.C. (1974) The determination of alkali metals in glasses by electron probe microanalysis. Glass Technology, 15, 123–126.

Hinton, R.W. (1990) Ion microprobe trace-element analysis of silicates—measurement of multi-element glasses. Chemical Geology, 83, 11–25.

Hovington, P., Drouin, D., and Gauvin, R. (1997) CASINO: A New Monte Carlo Code in C Language for Electron Beam Interaction. Part I: Description of the Program. Scanning, 19, 1–14.

Hulinsky, V., Jurek, K., and Gedeon, O. (1996) Experimental verification of theoretical models simulating the temperature increase in EPMA of glass. Mikrochimica Acta, Suppl. 13, 325–332.

Jambon, A. (1983) Diffusion dans les silicate fondus: un bilan des connaissances actuelles. Bulletin de Minéralogie, 106, 229–246.

Jbara, O., Cazaux, J., and Trebbia, P. (1995) Sodium diffusion in glasses during electron irradiation. Journal of Applied Physics, 78, 868–875.

Jones, G.O. (1971) Glass, 128 p. Chapman and Hall, Toronto.

Jurek, K., Hulinsky, V., and Gedeon, O. (1996) Electron beam induced migration of alkaline ions in silica glass. Mikrochimica Acta, [Suppl.] 13, 339–347.

Kanaya, K. and Okayama, S. (1972) Penetration and energy–loss theory of electrons in solid targets. Journal of Physics D: Applied Physics, 5, 43–58.

Kearns, S.L., Steen, N., and Erlund, E. (2002) Electronprobe microanalysis of volcanic glass at cryogenic temperatures. Microscopy and Microanalysis, 8, Suppl. 2, 1562CD.

King, P.L., Vennemann, T.W., Holloway, J.R., Hervig, R.L., Lowenstern, J.B., and Forneris, J.F. (2002) Analytical techniques for volatiles: A case study using intermediate (andesitic) glasses. American Mineralogist, 87, 1077–1089.

Lineweaver, J.L. (1963) Oxygen outgassing caused by the electron bombardment of glass. Journal of Applied Physics, 34, 1786.

Mandeville, C.W., Webster, J.D., Rutherford, M.J., Taylor, B.E., Timbal, A., and Faure, K. (2002) Determination of molar absorptivities for infrared absorption bands of H_2O in andesitic glasses. American Mineralogist, 87, 813–821.

Miotello, A. and Mazzoldi, P. (1982) Numerical analysis of field–assisted sodium migration in electron-irradiated glasses. Journal of Physics C: Solid State Physics, 15, 5615–5621.

Morgan, G.B. and London, D. (1996) Optimizing the electron microprobe analysis of hydrous alkali aluminosilicate glasses. American Mineralogist, 81, 1176–1185.

Morgan, G.B. and London, D. (2005) Effect of current density on the electron microprobe analysis of alkali aluminosilicate glasses. American Mineralogist, 90, 1131–1138.

Mysen, B.O. (1983) The structure of silicate melts. Annual Reviews of Earth and Planetary Sciences, 11, 75–97.

Nielsen, C.H. and Sigurdsson, H. (1981) Quantitative methods for electron microprobe analysis of sodium in natural and synthetic glasses. American Mineralogist, 66, 547–552.

Pouchou, J.L. and Pichoir, F. (1984) "PAP" (φ–ρ–z) correction procedure for improved quantitative microanalysis. In J.T. Armstrong, Ed., Microbeam Analysis, p. 104–106. San Francisco Press, California.

Shelby, J.E. (1997) Introduction to glass science and technology, 255 p. The Royal Society of Chemistry, Cambridge, England.

Spray, J.G. and Rae, D.A. (1995), Quantitative electron-microprobe analysis of alkali silicate glasses: A review and user guide. The Canadian Mineralogist, 33, 323–332.

Stolper, E. (1982) The speciation of water in silicate melts. Geochimica et Cosmochimica Acta, 46, 2609–2620.

Usher, D.M. (1981) Sodium ion migration in glass on electron beam irradiation. Journal of Physics C: Solid State Physics, 14, 2039–2048.

Vassamillet, L.F. and Caldwell, V.E. (1969) Electron-probe microanalysis of alkali metals in glasses. Journal of Applied Physics, 40, 1637–1643.

Zhang, Y. (1999) H_2O in rhyolitic glasses and melts: measurement, speciation, solubility and diffusion. Reviews of Geophysics, 37, 493–516.